PCCP

ARTICLE TYPE

Cite this: DOI: 00.0000/xxxxxxxxxx

Integrated protocol to study hydrogen abstraction reactions by atomic hydrogen in flexible molecules: Application to the butanol isomers†

David Ferro-Costas,*[a] M. Natália D.S. Cordeiro,[b] and Antonio Fernández-Ramos*[a]

Received Date
Accepted Date

DOI: 00.0000/xxxxxxxxxx

This work presents a protocol designed to study hydrogen abstraction reactions by atomic hydrogen in molecules with multiple conformations. The protocol starts with the search and location of the conformers of the equilibrium structures by the `TorsiFlex` program. By a simple modification of the starting geometry of reactants, a Python script generates the input for the hydrogen abstraction transition states. Initially, the search of the stationary points (reactants and transition states) is carried out at a low-level employing firstly a preconditioned search and secondly a random search. The low-level conformers were reoptimized at a higher level electronic structure method. This information allows the evaluation of the multistructural harmonic-oscillator partition functions, which are corrected for zero-point energy anharmonicity by the hybrid degeneracy-corrected second-order vibrational perturbation theory and for torsional anharmonicity by the multistructural torsional method, as implemented in the `MsTor` program. The structural information of the stationary points is employed by `Pilgrim` to evaluate the multipath canonical variational transition state theory thermal rate constants with multidimensional small-curvature corrections for tunneling. Therefore, the thermal rate constants include variational (recrossing) and tunneling effects in addition to the effect of multiple conformations on the thermal rate constants. These features grant the applicability of the method to a wide range of temperatures. The method was applied to each of the hydrogen abstraction sites of the four isomers of butanol. The methodology employed allowed us to calculate thermal rate constants in the temperatures range 250-2500 K and to accurately fit them to analytical expressions. The variety of the abstraction sites shows that the protocol is robust and that can be employed to study hydrogen abstraction reactions in molecules containing carbon and oxygen as heavy atoms.

1 Introduction

Hydrogen abstraction (HA) reactions by atomic hydrogen from alkanes, alkenes,[1] saturated and unsaturated oxygenated compounds[2,3] are prone to be classified into various classes. Such classification depends on the carbon and oxygen (in the case of oxygenated species) sites to which the abstracted hydrogen atom is attached. The most elementary reaction kinetics study for bimolecular reactions of this type, for instance by transition state theory,[4] needs structural information about the reactants and the transition states. Obtaining these stationary points is straightforward for middle sized polyatomic species lacking conformational freedom but is more involved for flexible unsaturated hydrocarbons and alcohols. For the latter, the accurate prediction of the thermochemical data requires accounting for all conformations that can be reached by internal rotations about single C-C and C-O bonds.[5–7] This problem is especially acute for high-temperature chemical processes, as is the case of combustion reactions.

The objective of this work is to study HA reactions by atomic hydrogen in a wide range of temperatures, not just at high temperatures, and these reactions present additional difficulties at temperatures below ca. 500 K. Specifically, at low temperatures quantum effects (tunneling) are of importance because of the transfer of the hydrogen atom that can penetrate the potential en-

[a] *Center for Research in Biological Chemistry and Molecular Materials (CIQUS), University of Santiago de Compostela, 15782, Santiago de Compostela, Spain.*
[b] *LAQV@REQUIMTE, Department of Chemistry & Biochemistry, Faculty of Sciences, University of Porto, Rua do Campo Alegre, 4169-007, Porto, Portugal.*
* Electronic mail: david.ferro@usc.es, qf.ramos@usc.es

† Electronic Supplementary Information (ESI) available: It includes the execution steps of all involved programs; the evolution of anharmonic factors, transmission coefficients and product branching ratios with temperature; the relative energy of the conformers of reactants and transition states; the MP-CVT/SCT rate constants and its components according to eqn (17); the MPWB1K/6-31+G(d,p) and F12-CCSD(T)/cc-PVTZ//MPWB1K/6-31+G(d,p) absolute energies and the barrier heights for eqn (2) obtained by the two methods; The variational an tunneling transmission coefficients of each TS conformer for each hydrogen abstraction channel; the fitting parameters to eqn (24); and the Cartesian coordinates and absolute energy of all the stationary point conformers (reactants and transition states) calculated at the MPWB1K/6-31+G(d,p) level. See DOI: 10.1039/cXCP00000x/

ergy barrier. This effect becomes negligible at high-temperatures, but then molecular flexibility and torsional anharmonicity may play a crucial role, so both effects need to be included.

Multipath[8–12] variational transition state theory[13,14] (MP-VTST) incorporates multidimensional quantum effects, variational effects, and the impact of multiple conformations on the reaction dynamics, so it can be employed to evaluate thermal rate constants in a wide range of temperatures. In this work, we apply the canonical version (CVT)[15,16] of multipath variational transition state theory with multidimensional small-curvature tunneling (SCT)[17,18] corrections (MP-CVT/SCT, hereafter) to evaluate the thermal rate constants in the temperature interval 250–2500 K of the HA reactions by atomic hydrogen of the four structural isomers of butanol (BuOH): 1-butanol or n-butanol (1-BuOH), 2-butanol (2-BuOH), isobutanol (i-BuOH), and tert-butanol (t-BuOH). Three of the four isomers present conformational isomers (except for t-BuOH) and the four of them contain HA transition states with several conformations. In this situation, it is convenient to adopt the concept of conformational reaction channel (CRC);[19,20] which is formed by the set of all HA transition states obtained from the same abstraction site that are conformational isomers, so they can interconvert between them by internal rotations about single bonds.

Therefore, with the objective of integrating conformational flexibility within the framework of MP-VTST, we have designed a protocol that combines three computer programs plus electronic structure software.

The protocol consists of: (i) search and location of the torsional conformers of the BuOH isomers and of the HA transition states for each CRC (ii) calculation of torsional anharmonicity (iii) evaluation of the rate constants and branching ratios using MP-CVT/SCT. Notice that MP-CVT/SCT is one of the most complete versions of MP-VTST because it includes quantum and variational effects, torsional anharmonicity, and conformational flexibility, but the protocol can also be applied to other versions of the theory that neglect one or several of the aforementioned improvements.

Recently, Elliott et al.[21] described a similar protocol to the one just mentioned, employing the `AutoMech`[22] program to study HA reactions from several alkanes and alcohols by small radicals at high temperatures. Specifically, to evaluate the thermal rate constants, they carried out one-dimensional scans to locate the conformers and incorporate tunneling effects through the Eckart barrier approximation.

For mechanisms with intricated reaction networks, the location of the TS structures may be arduous, so several codes with different levels of automatization have been developed to ease this task, as for instance, `AutoMech`,[22] `AutoMeKin`,[23] `AutoTST`,[24] `EsTokTP`,[25] `KinBot`,[26] `RMG`,[27] and TUMME.[28] However, the starting geometries for the TS structures of HA reactions by atomic hydrogen can be easily guessed, so this is not a relevant problem for these types of reactions. Instead, we focus our attention on features that are characteristic of hydrogen transfer reactions in flexible molecules.

The HA reactions studied in this work are labeled as R_Z^Y, where Z indicates the structural isomer of butanol (Z=1, 2, i, or t) and Y the abstraction site. The same nomenclature is used to distinguish among the corresponding transition states (TS_Z^Y) and radical species generated in the reaction (products, P_Z^Y). For 1-BuOH, they consist of five CRCs (see Fig. 1a):

$$R_1^O : \text{1-BuOH} + H^\bullet \rightarrow [TS_1^O]^\ddagger \rightarrow H_2 + P_1^O$$

$$R_1^\alpha : \text{1-BuOH} + H^\bullet \rightarrow [TS_1^\alpha]^\ddagger \rightarrow H_2 + P_1^\alpha \quad (\times 2)$$

$$R_1^\beta : \text{1-BuOH} + H^\bullet \rightarrow [TS_1^\beta]^\ddagger \rightarrow H_2 + P_1^\beta \quad (\times 2)$$

$$R_1^\gamma : \text{1-BuOH} + H^\bullet \rightarrow [TS_1^\gamma]^\ddagger \rightarrow H_2 + P_1^\gamma \quad (\times 2)$$

$$R_1^\delta : \text{1-BuOH} + H^\bullet \rightarrow [TS_1^\delta]^\ddagger \rightarrow H_2 + P_1^\delta$$

For 2-BuOH[‡] (Fig. 1b) there exist six different abstraction sites:

$$R_2^O : \text{2-BuOH} + H^\bullet \rightarrow [TS_2^O]^\ddagger \rightarrow H_2 + P_2^O$$

$$R_2^\alpha : \text{2-BuOH} + H^\bullet \rightarrow [TS_2^\alpha]^\ddagger \rightarrow H_2 + P_2^\alpha$$

$$R_2^\beta : \text{2-BuOH} + H^\bullet \rightarrow [TS_2^\beta]^\ddagger \rightarrow H_2 + P_2^\beta$$

$$R_2^{\beta'} : \text{2-BuOH} + H^\bullet \rightarrow [TS_2^{\beta'}]^\ddagger \rightarrow H_2 + P_2^{\beta'}$$

$$R_2^m : \text{2-BuOH} + H^\bullet \rightarrow [TS_2^m]^\ddagger \rightarrow H_2 + P_2^m$$

$$R_2^\gamma : \text{2-BuOH} + H^\bullet \rightarrow [TS_2^\gamma]^\ddagger \rightarrow H_2 + P_2^\gamma$$

Notice that there are two different C_β: the methylenic carbon (reaction labelled with the β and β' subscripts)[§] and the methylic one (m superscript).[29] Due to the chirality of the system, the two hydrogen atoms attached to the methylenic C_β are not energetically equivalent (in contrast to 1-butanol), leading to two different reaction channels (β and β') as shown in Fig. 1b.

For i-BuOH, we have considered the following four reaction channels (Fig. 1c):

$$R_i^O : \text{i-BuOH} + H^\bullet \rightarrow [TS_i^O]^\ddagger \rightarrow H_2 + P_i^O$$

$$R_i^\alpha : \text{i-BuOH} + H^\bullet \rightarrow [TS_i^\alpha]^\ddagger \rightarrow H_2 + P_i^\alpha \quad (\times 2)$$

$$R_i^\beta : \text{i-BuOH} + H^\bullet \rightarrow [TS_i^\beta]^\ddagger \rightarrow H_2 + P_i^\beta$$

$$R_i^\gamma : \text{i-BuOH} + H^\bullet \rightarrow [TS_i^\gamma]^\ddagger \rightarrow H_2 + P_i^\gamma \quad (\times 2)$$

Notice that the abstraction at methylenic carbons (1-BuOH and i-BuOH) leads to two CRCs with TSs that are configurational enantiomers. Consequently, only one CRC needs to be computed in these situations and the total rate constant can be just simply multiplied by a factor of two (indicated with $\times 2$).

Finally, for t-BuOH there are two channels (Fig. 1d):

$$R_t^O : \text{t-BuOH} + H^\bullet \rightarrow [TS_t^O]^\ddagger \rightarrow H_2 + P_t^O$$

$$R_t^\beta : \text{t-BuOH} + H^\bullet \rightarrow [TS_t^\beta]^\ddagger \rightarrow H_2 + P_t^\beta$$

The main interest of the above reactions is associated with combustion because three of the four isomers of butanol can be

‡ In this work we have considered the *S*-2-butanol steroisomer but the same applies to *R*-2-butanol.

§ For the H_β hydrogen the H_β-C_β-C_γ-C_α improper torsion is positive, whereas for $H_{\beta'}$ is negative.

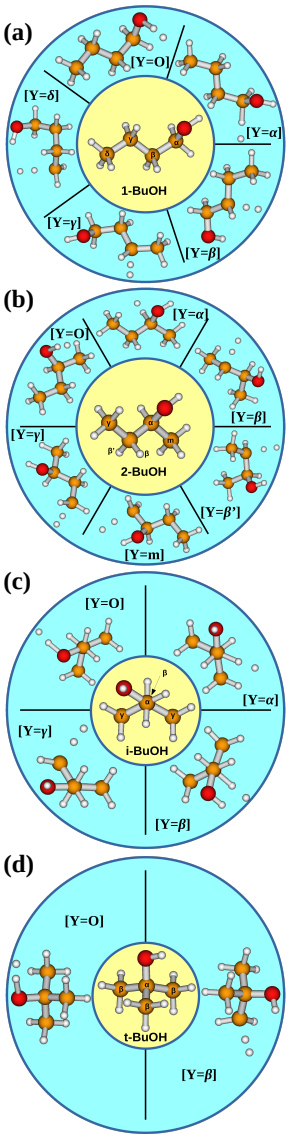

Fig. 1 Representative conformers of each butanol isomer (Z-BuOH, internal circle) and of each HA transition state. (a) Z = 1, (b) Z = 2, (c) Z=i and (d) Z = t. The abstraction site (Y) is also indicated for each transition state between squared brackets.

produced from biomass and therefore are considered biofuels.[30] The exception is tert-butanol, which still lacks a biological synthesis route. The combustion of biobutanol is characterized by a bevy of reactions.[31] During the initiation and chain branching reactions, several small radicals capable of abstracting hydrogen atoms (such as H, OH, CH_3 or HO_2) are generated. These initial steps are crucial in the early stages of combustion since they produce radicals that decompose further and maintain the combustion.

There are theoretical studies on the HA reactions on butanols by the hydroxyl radical[32,33], methyl radical[34] and by the HO_2 radical[35], but to the best of our knowledge, theoretical calculations involving atomic hydrogen are scarce. Ratkiewicz *et al.*[2] applied reaction-class transition state theory[36] to study several HA reactions by atomic hydrogen from several alcohols, including 1-butanol and 2-butanol. However, the approach is approximate in the sense that treats tunneling effects from a one-dimensional point of view and neglects the effect of multiple conformers; two aspects that are treated more rigorously in our protocol. From the experimental point of view, the data originate from kinetic model studies on combustion,[31,37–41] and therefore they are also approximate.

This work is organized as follows. Section 2 briefly describes MP-CVT/SCT. Section 3 provides information about the computational protocol. Section 4 presents the results and discussion. Finally, Section 5 summarizes the main conclusions of this work.

2 Theory

According to transition state theory (TST), the rate constant of a bimolecular reaction:[4]

$$\mathrm{A} + \mathrm{B} \rightarrow [\mathrm{TS}] \rightarrow \mathrm{Product(s)} \tag{1}$$

is given by:

$$k^{\mathrm{TST}}(T) = \frac{1}{h\beta}\frac{Q_{\ddagger}(T)}{Q_{\mathrm{A}}(T)\cdot Q_{\mathrm{B}}(T)}e^{-\beta V_0} \tag{2}$$

where β is the inverse of the product of Boltzmann's constant and the temperature (T), h is Planck's constant, Q_{A} and Q_{B} are the partition functions of the reactants, $Q_{\ddagger}$ is the partition function of the transition state and V_0 is the energy difference between the transition state and the reactants. Partition functions and rate constants are temperature-dependent but hereinafter, and for the sake of simplicity, we will drop this dependence.

The total partition function can be expressed as a product of translational (Q_{tr}), rovibrational (Q_{rv}) and electronic (Q_{el}) contributions:

$$Q = Q_{\mathrm{tr}}\cdot Q_{\mathrm{rv}}\cdot Q_{\mathrm{el}} \tag{3}$$

Regarding the rovibrational partition function, the most common approximation is based on the separation of the rotational and vibrational movements through the rigid-rotor (RR) and harmonic oscillator (HO) models:

$$Q_{\mathrm{rv}}^{\mathrm{RRHO}} = Q_{\mathrm{rot}}^{\mathrm{RR}}\cdot Q_{\mathrm{vib}}^{\mathrm{HO}} \tag{4}$$

It is frequent to adopt the quasiharmonic (QH) approximation that incorporates a scaling factor to the harmonic vibrational frequencies.[42,43] In this work, instead of considering the same factor for scaling the vibrational frequencies of reactants and transition states, we have opted for an approach that scales them by a factor $\lambda_{\mathrm{X}}^{\mathrm{ZPE}}$, which is evaluated as:[44]

$$\lambda_{\mathrm{X}}^{\mathrm{ZPE}} = \lambda_{\mathrm{X}}^{\mathrm{H}}\cdot\lambda_{\mathrm{X}}^{\mathrm{anh}} \tag{5}$$

being X = R (reactants) or X=‡ (transition state). Notice that the difference between $Q_{\mathrm{vib}}^{\mathrm{HO}}$ and its QH version, $Q_{\mathrm{vib}}^{\mathrm{QH}}$, is that for the former $\lambda_{\mathrm{X}}^{\mathrm{ZPE}} = 1$. The scaling factor λ^{H} is tabulated for a large number of electronic structure methods and accounts for the inexactness of the electronic model chemistry, and therefore it is the same for R and TS.[44] The anharmonic $\lambda_{\mathrm{X}}^{\mathrm{anh}}$ factor is computed by the hybrid degeneracy-corrected[45] second-order vibrational perturbation theory[46] (HDCVPT2). In this manner, a different $\lambda_{\mathrm{X}}^{\mathrm{anh}}$

factor is obtained for different stationary points.

Equation (2) can be generalized using variational transition state theory[13,14] that, through a transmission coefficient, accounts for recrossing and tunneling effects. Within the canonical approximation (CVT) and within the SCT correction for tunneling, the thermal rate constant is given by:

$$k^{\mathrm{CVT/SCT}} = \gamma^{\mathrm{CVT/SCT}} \cdot k^{\mathrm{TST}} \tag{6}$$

with

$$\gamma^{\mathrm{CVT/SCT}} = \Gamma^{\mathrm{CVT}} \cdot \kappa^{\mathrm{CVT/SCT}} \tag{7}$$

where Γ^{CVT} is the ratio between the CVT and TST thermal rate constants and $\kappa^{\mathrm{CVT/SCT}}$ is the SCT transmission coefficient. Whereas the evaluation of the TST rate constant only requires a detailed knowledge of the reactants and the transition state, the CVT/SCT rate constant needs information along the minimum energy path (MEP). Equation (7) has shown to perform well against accurate quantum dynamics calculations performed for atom-diatom reactions[47] and for polyatomic system reactions[48]. However, eqn (7) needs adjustments when dealing with multiple conformers. These modifications are described below.

Multiple conformations and torsional anharmonicity

The rovibrational partition function should be adapted to incorporate the rotational conformers. The simplest approximation consists on summing over all the individual partition functions where vibrations are treated quasiharmonically (SS-QH). This is known as the multi-structural quasiharmonic oscillator approximation (MS-QH), and the corresponding partition function is given by:

$$Q_{\mathrm{rv,X}}^{\mathrm{MS-QH}} = \sum_{j=0}^{N_{\mathrm{X}}-1} Q_{\mathrm{rv},j_{\mathrm{X}}}^{\mathrm{SS-QH}} e^{-\beta U_{j_{\mathrm{X}}}} \tag{8}$$

where N_{X} is the number of conformers (X=R or X=‡), $Q_{\mathrm{rv},j_{\mathrm{X}}}^{\mathrm{SS-QH}}$ is the single-structure partition function of the j_{X}-th conformer ($j_{\mathrm{X}} = 0$ represents the conformer with the lowest energy). In particular, $U_{j_{\mathrm{X}}}$ is the relative energy of the j_{X}-th conformer with respect to the most stable one. For convenience, the energies are sorted in increasing order:

$$U_{0_{\mathrm{X}}} \leq U_{1_{\mathrm{X}}} \leq \cdots \leq U_{N_{\mathrm{X}}-2} \leq U_{N_{\mathrm{X}}-1} \tag{9}$$

In view of eqn (8), it is also possible to define the contribution of the j_{X}-th conformer to the total MS-QH partition function, $\chi_{j_{\mathrm{X}}}$, which can be calculated as:

$$\chi_{j_{\mathrm{X}}}^{\mathrm{QH}} = \frac{Q_{\mathrm{rv},j_{\mathrm{X}}}^{\mathrm{SS-QH}}}{Q_{\mathrm{rv,X}}^{\mathrm{MS-QH}}} e^{-\beta U_{j_{\mathrm{X}}}} \tag{10}$$

The multistructural version of the transition state theory (MS-TST) rate constant can be written as a product of two magnitudes:

$$k^{\mathrm{MS-TST}} = F^{\mathrm{MS-T}} \cdot k^{\mathrm{SS-TST}} \tag{11}$$

One of them, $k^{\mathrm{SS-TST}}$, is the rate constant of eqn (2), evaluated considering the lowest-energy conformer for both the reactant and the transition state ($j_{\mathrm{X}} = 0$). The other one, $F^{\mathrm{MS-T}}$, is the multistructural torsional (MS-T) factor, defined by the ratio between a MS-T factor at the transition state and at the reactants

$$F^{\mathrm{MS-T}} = \frac{F_{\ddagger}^{\mathrm{MS-T}}}{F_{\mathrm{R}}^{\mathrm{MS-T}}} \tag{12}$$

For both stationary points, each individual MS-T factor is given by the product of two different contributions:

$$F_{\mathrm{X}}^{\mathrm{MS-T}} = F_{\mathrm{X}}^{\mathrm{MS-QH}} \cdot F_{\mathrm{X}}^{\mathrm{T}} \tag{13}$$

The first one accounts for the influence of the conformations within the QH approximation:

$$F_{\mathrm{X}}^{\mathrm{MS-QH}} = \frac{Q_{\mathrm{rv,X}}^{\mathrm{MS-QH}}}{Q_{\mathrm{rv},j_{\mathrm{X}}=0}^{\mathrm{SS-QH}}} \tag{14}$$

and the second contribution incorporates torsional anharmonicity to the MS-QH partition functions:

$$F_{\mathrm{X}}^{\mathrm{T}} = \frac{Q_{\mathrm{rv,X}}^{\mathrm{MS-T}}}{Q_{\mathrm{rv,X}}^{\mathrm{MS-QH}}} \tag{15}$$

where $Q_{\mathrm{rv,X}}^{\mathrm{MS-T}}$ is calculated by means of the MS-T approximation, which considers the coupling among the different torsional modes.[5,7]

MP-CVT/SCT with torsional anharmonicity

At this point, there are two ways of improving over the MS-TST assumptions. The simplest way is to assume that the variational and quantum effects obtained starting from all transition state conformations are well represented by $\gamma_0^{\mathrm{CVT/SCT}}$, the transmission coefficient obtained from the MEP that starts at the transition state conformer with the lowest energy. This approximation is called mutistructural CVT/SCT (MS-CVT/SCT)[49] and its rate constant is given by:

$$k^{\mathrm{MS-CVT/SCT}} = \gamma_0^{\mathrm{CVT/SCT}} \cdot k^{\mathrm{MS-TST}} \tag{16}$$

where $k^{\mathrm{MS-TST}}$ is the multistructural transition state thermal rate constant, related to the single structure TST rate constant by eqn (11).

If the MEP is calculated starting from each of the transition state structures, the transmission coefficient is calculated as an average of all the $\gamma_{j_{\ddagger}}^{\mathrm{CVT/SCT}}$ contributions from all paths. This is the MP-CVT/SCT approximation and the thermal rate constant is given by:

$$k^{\mathrm{MP-CVT/SCT}} = F^{\mathrm{MS-T}} \cdot \langle\gamma\rangle^{\mathrm{CVT/SCT}} \cdot k^{\mathrm{SS-TST}} \tag{17}$$

where $k^{\mathrm{SS-TST}}$ is the single structure TST rate constant and

$$\langle\gamma\rangle^{\mathrm{CVT/SCT}} = \sum_{j_{\ddagger}} \Gamma_{j_{\ddagger}}^{\mathrm{CVT}} \cdot \kappa_{j_{\ddagger}}^{\mathrm{SCT}} \cdot \chi_{j_{\ddagger}}^{\mathrm{QH}} \tag{18}$$

where $\Gamma_{j_{\ddagger}}^{\mathrm{CVT}}$ and $\kappa_{j_{\ddagger}}^{\mathrm{SCT}}$ are the variational and tunneling contributions, respectively, of the $j_{\ddagger}$ conformer, and $\chi_{j_{\ddagger}}^{\mathrm{QH}}$ is given by eqn (10).

3 Computational protocol

This Section describes the current protocol, as well as possible extensions to adapt it to hydrogen abstraction reactions.

Current protocol

The evaluation of the multipath thermal rate constants follows the protocol shown in Fig. 2 as anticipated in the Introduction Section. The first stage is the search and location of the stationary points. This task is carried out by `Torsiflex`[50,51], a program written in Python 3 that requires as input an initial structure of the molecule in Z-Matrix format to start the conformational search. The torsions of interest specified in the Z-Matrix should be defined univocally, so the program can rotate them automatically. In this case one initial structure with this characteristics was generated for each butanol isomer.

`Torsiflex` starts an exploration of the torsional PES; usually, at an inexpensive level of theory. In this case this search was carried out at the HF/3-21G level.[52] First, `Torsiflex` employs a preconditioned algorithm that performs a systematic search based on chemical knowledge. For molecules with torsional enantiomers (for instance, 1-butanol), `Torsiflex` automatically takes them into account. For the isomers of butanol the expected number of new conformers generated applying this algorithm is three for each torsion (one *anti* and two *gauche* configurations). In a second round, `Torsiflex` performs a random search with the objective of locating conformers outside of the region already explored by the preconditioned algorithm. The number of random trial geometries is specified by the user. If the optimization of a given stationary point succeeds, the Hessian matrix is computed to confirm that the geometry corresponds to an equilibrium structure.

All the stored HF/3-21G optimized conformations were further reoptimized at the MPWB1K density functional theory (DFT) level[53] with the 6-31+G(d,p) basis set.[54] MPWB1K has been specifically parametrized for kinetics and thermochemistry[55] and it was already benchmarked against several high-level *ab initio* methods for this kind of reactions.[56] With the object of refining even further the HA barrier heights, single-point energy calculations over the MPWB1K geometries were performed for the lowest energy conformer of each CRC at the F12-CCSD(T)[57] level with the cc-pVTZ[58] basis set. All electronic structure calculations were carried out with the *Gaussian09* package[59] except for the single point F12-CCSD(T) calculations that were performed with Orca.[60]

The TS-like initial structures in Z-Matrix format were built from those of the initial geometries for the equilibrium structures. It implies the generation of one initial geometry for each CRC, that is, 6 structures for 2-BuOH, 4 for i-BuOH, 5 for i-BuOH and 2 for t-BuOH, leading to a total of 17 structures. This task is carried out by the Python script listed in the ESI that generates the template for the geometries. It works as follows:

- Gets the adjacency matrix of the system (a matrix that indicates the molecular connectivity) to identify the connectivity of the TSs.
- Identifies, for each heavy atom, Y_1, a bonded hydrogen (H-Y_1 bond). In the case of 2-BuOH, the two β hydrogen atoms have different chemical environment, so both of them need to be included.
- Continues along the heavy atoms chain and locates a second heavy atom, Y_2, bonded to Y_1 (H-Y_1-Y_2 bent angle).
- Adds a dummy atom (Bq) with fixed H-Y_1 distance, Bq-H-Y_1 angle, and Bq-H-Y_1-Y_2 dihedral angle, and values of 1 Å, 90°, and 0°, respectively.
- Adds the $H^\bullet$ radical to the Z-Matrix considering the $H^\bullet$-H-Bq-Y_1 dihedral angle.

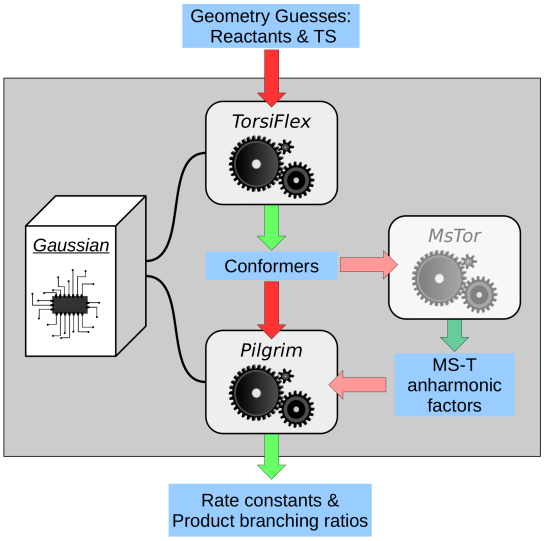

Fig. 2 Procedure followed in the study of HA reactions for systems with conformational flexibility.

The resulting template is the reference structure for `Torsiflex`. As in the case of butanol isomers, HF/3-21G was the selected electronic structure method employed for the location of TS conformations. This level of calculation tends to produce tighter transitions states than DFT methods, easing the optimization. It also produces reasonable structures for hydrogen transfer reactions -probably due to error compensation, and in the past it was adopted to parametrize semiempirical methods.[61]

In the above algorithm, the H-H, and H-Y_1 distances, as well as the H-H-Y_1 bent angle need initial values. These three geometrical parameters depend on the nature of the donor and acceptor atoms. In general, H abstraction reactions by atomic hydrogen usually present linear or close to linear H-H-Y_1 angles, so the starting angle for optimization is 180°. For the H-H and H-Y_1 distances we have chosen initial values of 1.03 and 1.37 Å, respectively, when Y_1 is a carbon atom and 0.90 and 1.25 Å when Y_1 is oxygen. All TS optimizations starting from the template were successful, leading to an optimized TS structure for each CRC. `TorsiFlex` performs a Hessian calculation to warrant that the optimized structure is a first-order saddle point. Additionally, the program has some extra criteria to decide whether the saddle-point corresponds to the desired TS or to a TS of a different reaction coordinate (for instance, to a hindered rotor TS).

For each abstraction site, `TorsiFlex` employs the final parameters of the reference optimized geometry in the seek for other TS conformers. `TorsiFlex` search for the next possible conformer near this first optimized structure employing the preconditioned algorithm. The procedure continues until the set of preconditioned torsional angles is exhausted. Next, the program performs a stochastic search having as framework the previous conformational network. Once the conformational search is completed, a reoptimization of the TS structures is carried out at the MPWB1K level. If the optimization is successful, Hessian calculations are performed to ensure that the TSs correspond to the reactions of interest.

Additionally, `TorsiFlex` performs a series of tests for each optimized geometry, i.e., a connectivity test (that ensures that the initial and final species are the same), redundancy test (that avoids redundant structures), and a constraints test (that excludes structures outside the constraints specified by the user).

For each CRC, ZPE anharmonicity can be included through specific reaction scaling factors for frequencies by performing an additional HDCVPT2 calculation at the MPWB1K/6-31+G(d,p) level for the geometry with the lowest energy. For that purpose we have employed the *Gaussian09* package. If the standard scaling factors are employed this step is omitted.

Torsional anharmonicity is incorporated through the multistructural torsional factor with explicit potential coupling of torsions [MS-T(C) or MS-T for short].[7] This procedure includes couplings between the torsions and between the torsions and the rest of degrees of freedom. This method was previously applied to a set of twenty molecules having two hindered rotors and compared with extended two dimensional torsional (E2DT) method that takes into account quantum effects and full coupling between the torsional modes.[62–64] For these types of systems, MS-T showed to be an adequate alternative to E2DT. Taking into account that E2DT cannot be applied to molecules with more than two torsions, MS-T is our choice for including torsional anharmonicity. Additionally, the evaluation of MS-T just needs information of the stationary points, which makes it affordable for systems with multiple torsions.

The torsional factor of eqn (13) with the ZPE scaling factors were evaluated by the `MSTor` program.[65,66] The input file for MSTor can be built by executing the utility files distributed with the program, but it can also be automatically generated by `TorsiFlex`. This input file is unique for each set of conformers, i.e., there are four input files (one for each butanol isomer) plus 17 input files that account for all types of TS structures, as mentioned earlier.

The output files generated by `TorsiFlex` and by `MSTor` are read by `Pilgrim`.[67] This program coded in Python 3 is responsible for the thermal rate constant calculations, and it can produce several flavors of VTST, that is, SS-TST, MS-TST, SS-CVT, MS-CVT, MP-CVT, plus versions of these rate constants including zero-curvature tunneling (ZCT)[68] and SCT.[17,18] Of all of them, the most complete is MP-CVT/SCT, which is also used as benchmark along this work. The evaluation of the MP-CVT/SCT thermal rate constants requires following the MEP for each individual TS, and the $\gamma_{j_\ddagger}^{\mathrm{CVT/SCT}}$ transmission coefficients were obtained from information extracted from these paths. In particular, each MEP was followed using the Page-McIver algorithm[69] with a cubic first step of 10^{-4} Bohr and further steps of 0.005 Bohr with Hessian calculations every 10 steps. Redundant internal coordinates were automatically generated by `Pilgrim` and employed to extract the projected normal mode frequencies along the MEP.[70] Each MEP was automatically extended until the corresponding κ^{SCT} tunneling transmission coefficient converged within an error smaller than 0.5%.

All points along the MEP were obtained using the MPWB1K/6-31+G(d,p) level (hereafter DFT or MPWB1K); however, the DFT thermal rate constants for each CRC were corrected with F12-CCSD(T)/cc-pVTZ//MPWB1K/6-31+G(d,p) single point calculations (hereafter F12). Specifically, for each CRC, all energy differences between conformers, and variational and tunneling effects were calculated at the DFT method except the barrier height, V_0, of the SS-TST thermal rate constant [see eqns (2) and (17)] that was evaluated at the F12 level. Therefore, the barrier height between a reactants conformer j and a TS conformer $j_\ddagger$ within a CRC, which at the DFT level is given by $U_j^{\mathrm{DFT}} + V_0^{\mathrm{DFT}} + U_{j_\ddagger}{}^{\mathrm{DFT}}$, is now given by $U_j^{\mathrm{DFT}} + V_0^{\mathrm{F12}} + U_{j_\ddagger}{}^{\mathrm{DFT}}$.

A sorted sequence with the commands employed to execute each of the programs is provided in the ESI.

Protocol extension

The above protocol can be also employed to study HA reactions from the methyl (CH_3), hydroxyl (OH), and hydroperoxyl (HOO) radicals. In the case of methyl radicals the template would be almost identical to the one described above because the Y_1-H-CH_3 angle at the transition state structure is close to linearity.[71,72] On the contrary, the Y_1-H-OH angle can be highly bent (valence angle smaller than 150°) due to the possibility of H-bond formation of the OH radical with atoms of the other molecule.[33] In this case, it would be better to define in the template an interval for the generation of the trial set {$Y_1\cdots$H, H$\cdots$O, Y_1-H-OH}, and if the TS optimization fails a different trial set is generated within the previously defined interval. Additionally, the template should include the Y_2-Y_1-O-H dihedral, which may also lead to different conformers. For the case of HOO, the procedure would be similar to the OH case, but including an additional dihedral angle.

For the case of unimolecular reactions (for instance, decomposition, or isomerization reactions), instead of a template for building the initial geometry of the TS, it is better to operate with programs that generate reaction networks, as for instance the ones cited in the Introduction Section. In this context, we are preparing an interface between `Torsiflex`, `Pilgrim`, and AutoMeKin.[23] For these reactions the protocol will be similar to the one employed by some of us in the study of the decomposition of the 1-propanol radical[20] but incorporating multistructural and anharmonic effects through the combination `Torsiblex`, `MsTor` instead of through the `Q2DTor` program.[64]

4 Results and Discussion

In this Section we describe the procedure to obtain the MP-CVT/SCT rate constants for the HA reactions from atomic hydro-

gen for the four isomers of butanol.

Conformational search

In order to distinguish among the different conformers, we need to define the nomenclature used to classify a given torsion angle (ϕ_i). We followed the International Union of Pure and Applied Chemistry (IUPAC) recommendations adding some intermediate cases, as proposed by Truhlar and coworkers,[73] (in lowercase letters):

- **C** if $\phi_i = 0°$
- $\mathbf{C}^-$ if $\phi_i \in (-30°, 0°)$ and $\mathbf{C}^+$ if $\phi_i \in (0°, +30°)$
- $\mathbf{G}^-$ if $\phi_i \in (-75°, -30°)$ and $\mathbf{G}^+$ if $\phi_i \in (+30°, +75°)$
- $\mathbf{g}^-$ if $\phi_i \in (-90°, -75°)$ and $\mathbf{g}^+$ if $\phi_i \in (+75°, +90°)$
- $\mathbf{a}^-$ if $\phi_i \in (-105°, -90°)$ and $\mathbf{a}^+$ if $\phi_i \in (+90°, +105°)$
- $\mathbf{A}^-$ if $\phi_i \in (-150°, -105°)$ and $\mathbf{A}^+$ if $\phi_i \in (+105°, +150°)$
- $\mathbf{T}^-$ if $\phi_i \in (-180°, -150°)$ and $\mathbf{T}^+$ if $\phi_i \in (+150°, +180°)$
- **T** if $\phi_i = 180°$

For the systems here studied, when labelling a given conformer, we start from the O-side of the chain and move by one bond along the chain. For all isomers of BuOH, the first dihedral is $HO-C_\alpha C_\beta$. Except for t-BuOH, for which there is only one dihedral that may lead to distinguishable structures, the second dihedral is defined as $OC_\alpha - C_\beta C_\gamma$. Finally, in the case of 1-BuOH the third dihedral is defined as $C_\alpha C_\beta - C_\gamma C_\delta$. Notice that the rotation of the methyl group produces structures that are indistinguishable, but it should be included later on when dealing with torsional anharmonicity. Conformational energies of the equilibrium structures are listed in Table 1. In the case of the transition states this information is given in the ESI.

The expected number of new conformers generated by each torsion is three and, therefore, the number of expected structures scales as 3^t, being t the number of torsions that produce distinguishable conformers. However, there are molecules, as for instance 1-BuOH, that present conformational enantiomerism; in these cases the search can be reduced to $\frac{1}{2}(3^t+1)$ instead of 3^t structures.

For the molecules studied here, which do not present important intramolecular interactions or strong torsional coupling, the resulting conformers deviate only slightly from the expected torsions (see Table 2). However, there are cases, as the structure $\mathbf{G}^+\mathbf{G}^-\mathbf{a}^+$ of 1-butanol (and its enantiomer $\mathbf{G}^-\mathbf{G}^+\mathbf{a}^-$), that involves torsional angles: $HO-C_\alpha C_\beta = +70°$, $OC_\alpha - C_\beta C_\gamma = -60°$, and $C_\alpha C_\beta - C_\gamma C_\delta = +91°$, in which one of the torsions deviated substantially from the anti (**T**) or gauche ($\mathbf{G}^+$, $\mathbf{G}^-$) configurations. Our results are in agreement with the calculations of Ohno *et al.*[74] that indicate that the **TGT** conformation is the one with the lowest energy.

Regarding the transition state conformers, the biggest discrepancy between the expected and located number of conformers can

Table 1 Relative MPWB1K energies (U_j) with respect to the most stable structure of each isomer of BuOH. Last column includes the ZPE contributions (within the QH approximation). Conformational enantiomers are omitted.

Isomer	Structure	U_j	U_j + ΔZPE
1-BuOH	$\mathbf{T}^-\mathbf{G}^+\mathbf{T}^-$	0.00	0.00
	$\mathbf{G}^+\mathbf{G}^+\mathbf{T}^-$	0.21	0.22
	TTT	0.28	0.20
	$\mathbf{G}^+\mathbf{T}^+\mathbf{T}$	0.29	0.28
	$\mathbf{G}^-\mathbf{G}^+\mathbf{T}^+$	0.30	0.35
	$\mathbf{T}\mathbf{G}^+\mathbf{G}^+$	0.42	0.54
	$\mathbf{G}^+\mathbf{G}^+\mathbf{G}^+$	0.62	0.74
	$\mathbf{G}^-\mathbf{G}^+\mathbf{G}^+$	0.83	0.99
	$\mathbf{G}^+\mathbf{T}^-\mathbf{G}^-$	0.96	1.05
	$\mathbf{T}^+\mathbf{T}^+\mathbf{G}^+$	0.98	1.02
	$\mathbf{G}^+\mathbf{T}^+\mathbf{G}^+$	1.06	1.13
	$\mathbf{T}^+\mathbf{G}^+\mathbf{G}^-$	1.55	1.55
	$\mathbf{G}^+\mathbf{G}^+\mathbf{G}^-$	1.59	1.65
	$\mathbf{G}^-\mathbf{g}^+\mathbf{G}^-$	2.01	2.22
	$\mathbf{G}^+\mathbf{G}^-\mathbf{a}^+$	2.47	2.63
2-BuOH	$\mathbf{T}^-\mathbf{G}^+$	0.00	0.00
	$\mathbf{G}^-\mathbf{G}^+$	0.18	0.14
	$\mathbf{G}^+\mathbf{G}^+$	0.32	0.29
	$\mathbf{G}^-\mathbf{T}^+$	0.47	0.53
	$\mathbf{T}^+\mathbf{T}^+$	0.56	0.58
	$\mathbf{G}^+\mathbf{T}^+$	0.76	0.77
	$\mathbf{G}^-\mathbf{G}^-$	0.79	0.94
	$\mathbf{T}^+\mathbf{G}^-$	0.79	0.91
	$\mathbf{G}^+\mathbf{G}^-$	1.21	1.34
i-BuOH	$\mathbf{T}^+\mathbf{G}^-$	0.00	0.00
	$\mathbf{G}^-\mathbf{G}^-$	0.11	0.14
	$\mathbf{G}^+\mathbf{G}^-$	0.24	0.23
	$\mathbf{T}\mathbf{G}^+$	0.30	0.38
	$\mathbf{G}^+\mathbf{G}^+$	0.48	0.61

Table 2 Number of torsions (t), number of expected conformers ($M = 3^t$), and total number of obtained conformers, N. The barrier height (in kcal/mol), V_0, between the reactant and the TS with the lowest energy is also indicated. Conformational TSs possessing torsional enantiomers are indicated with an asterisk (*).

System		t	M	N	V_0^{DFT}	V_0^{F12}
1-BuOH	*	3	27	29		
TS_1^{α}		3	27	19	6.37	6.87
TS_1^{β}		3	27	28	9.05	8.85
TS_1^{γ}		3	27	28	8.49	8.49
TS_1^{δ}	*	4	81	81	10.87	10.67
TS_1^{O}	*	3	27	23	12.37	13.82
2-BuOH		2	9	9		
TS_2^{α}		2	9	6	4.87	5.32
TS_2^{β}		2	9	9	8.93	8.83
$TS_2^{\beta'}$		2	9	9	9.19	9.15
TS_2^{m}		3	27	26	11.49	11.27
TS_2^{γ}		3	27	26	11.14	10.94
TS_2^{O}		2	9	9	12.44	13.81
i-BuOH	*	2	9	9		
TS_i^{α}		2	9	6	6.54	6.89
TS_i^{β}	*	2	9	9	6.52	6.74
TS_i^{γ}		3	27	27	11.29	10.99
TS_i^{O}	*	2	9	9	12.19	13.67
t-BuOH	*	0	1	1		
TS_t^{β}	*	2	9	9	11.62	11.32
TS_t^{O}	*	0	1	1	12.59	13.89

be found in the abstraction at the C_α carbon atom. The arrangement in which the H···H-C_α-OH moiety is about 180° does not lead to a conformational minimum. This fact is already known for this abstraction site[19,75] and, considering it beforehand, the number of expected conformers for the HA at C_α should be estimated by $2\cdot 3^{t-1}$, which leads to a better agreement with the number of located conformers. Their relative energies and geometries are listed in the ESI and the distribution of the TSs energies with respect to those of reactants is given in Fig. 3. As expected, the HA at the C_α carbon atom presents the smallest barrier height in all biobutanol isomers, although the energy of the TS_2^{α} is smaller than in the other cases, because the abstracted hydrogen atom is bonded to a secondary carbon atom. On the other hand, abstraction reactions from the OH and methyl groups (primary carbon atom) lead to the highest barrier heights.

Table 2 lists the V_0 barrier heights calculated by the MPWB1K and F12 methods, corroborating the good performance of this DFT method. Specifically, MPWB1K provides close results to the benchmark F12 calculations although, in general, slightly underestimates (by about 10%) the barrier heights. A similar F12 correction over MPWB1K was carried out by some of us in the study of the proton transfer of urea derivatives at low temperatures, which led to a good comparison between the calculated and experimental rate constants.[76] Therefore, here we employ a similar combination of methods to study HA reactions.

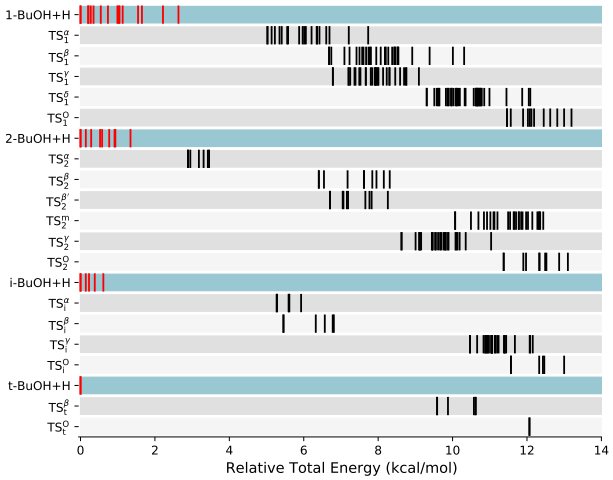

Fig. 3 Relative energy distribution (including the ZPE) of the reactants (red) and transition state (black) conformers for the HA channels. The reference energy was taken as that of the lowest energy conformer for the corresponding butanol isomer with the H atom infinitely separated.

Multiple structures and anharmonicity

We have considered two types of anharmonicity: (i) ZPE anharmonicity and (ii) torsional anharmonicity. Tradicionally, the former is handled by using a parametrized scaling factor, λ^{ZPE}, which in the case of the MPWB1K/6-31G(d,p) level has a value of 0.951.[77] However, the standard scaling factors are parametrized using databases containing small, stable molecules and, therefore, these factors may not be adequate to correct the ZPE of transition states or large equilibrium structures. Zero-point energy anharmonicity is calculated as the product of two factors, as indicated in eqn (5). The λ^{H} factor that includes the inexactness of the electronic structure method is taken from a database, and equals 0.964. However, the anharmonicity factor, λ^{anh}, is calculated by the HDCVPT2 method. This procedure seems suitable for these types of reactions;[78] Zheng *et al.*[79] applied this procedure and found that ZPE anharmonicity played a crucial role in the determination of branching ratios for the HA reaction from i-BuOH by the OH radical.

In this work, we have performed HDCVPT2 calculations for the lowest energy conformer of each of the reactants and transition states of each CRC (see Table 3). Notice that other way of writing eqn (5) is

$$\lambda^{\mathrm{ZPE}} = \lambda^{\mathrm{H}} \cdot \frac{\varepsilon_{\mathrm{ZPE}}^{\mathrm{anh}}}{\varepsilon_{\mathrm{ZPE}}^{\mathrm{HO}}} \tag{19}$$

where $\varepsilon_{\mathrm{ZPE}}^{\mathrm{HO}}$ and $\varepsilon_{\mathrm{ZPE}}^{\mathrm{anh}}$ are the harmonic and anharmonic ZPEs, respectively. In general, the λ^{ZPE} factor is close to the parametrized scaling factor of 0.951, but tend to be smaller than this value for the transition states, except for TS_i^{β}, TS_i^{γ}, and TS_2^{m}. The influence of this factor directly affects the vibrationally adiabatic potential, $V_a^{\mathrm{G}}(s)$, along the reaction coordinate, s, because

$$V_a^{\mathrm{G}}(s) = V_{\mathrm{MEP}}(s) + \varepsilon^{\mathrm{G}}(s) \tag{20}$$

Table 3 Harmonic and anharmonic zero point energy (kcal/mol) and the resulting λ^{ZPE} scale factor for the structure with the lowest energy within a given CRC. In all cases $\lambda^{\mathrm{H}} = 0.964$.

System	$\varepsilon_{\mathrm{ZPE}}^{\mathrm{HO}}$	$\varepsilon_{\mathrm{ZPE}}^{\mathrm{anh}}$	λ^{ZPE}
1-BuOH	88.33	87.13	0.951
TS_1^{α}	86.77	85.20	0.947
TS_1^{β}	86.60	84.91	0.945
TS_1^{δ}	87.11	85.95	0.951
TS_1^{γ}	86.54	85.39	0.951
$\mathrm{TS}_1^{\mathrm{O}}$	86.22	84.67	0.947
2-BuOH	87.85	87.09	0.956
TS_2^{α}	86.30	84.56	0.945
TS_2^{β}	86.24	84.64	0.946
$\mathrm{TS}_2^{\beta'}$	86.30	84.62	0.945
$\mathrm{TS}_2^{\mathrm{m}}$	86.27	85.89	0.960
TS_2^{γ}	86.20	84.73	0.948
$\mathrm{TS}_2^{\mathrm{O}}$	85.80	84.67	0.951
i-BuOH	87.97	86.55	0.948
$\mathrm{TS}_{\mathrm{i}}^{\alpha}$	86.46	84.96	0.947
$\mathrm{TS}_{\mathrm{i}}^{\beta}$	86.14	85.27	0.954
$\mathrm{TS}_{\mathrm{i}}^{\gamma}$	86.34	86.05	0.961
$\mathrm{TS}_{\mathrm{i}}^{\mathrm{O}}$	85.84	84.44	0.948
t-BuOH	87.22	86.05	0.951
$\mathrm{TS}_{\mathrm{t}}^{\beta}$	85.75	84.20	0.947
$\mathrm{TS}_{\mathrm{t}}^{\mathrm{O}}$	85.41	84.18	0.950

where $V_{\mathrm{MEP}}(s)$ is the potential along the MEP and $\varepsilon^{\mathrm{G}}(s)$ is the ZPE of the transverse modes to the reaction coordinate. The vibrationally adiabatic potential depends on the ZPE, and it is a key quantity in variational transition state theory affecting variational and tunneling effects; there the importance of having reliable scaling factors for the stationary points. Very recently, it has been encountered that a reaction-coordinate scaling-factor dependent $\lambda^{\mathrm{ZPE}}(s)$ improved the comparison with experiment in reactions occuring at ultra-low temperatures[76] and in reactions especially sensitive to tunneling and ZPE changes.[80] However, for the HA reactions studied in this work we follow the same procedure as in the study by Zheng *et al.*[79] for similar reactions with bioalcohols, that is, the vibrationally adiabatic potentials along the MEPs for a given set of conformers was scaled by a common λ^{ZPE} value obtained for the TS with the lowest energy (see Table 3).

The influence of the number of conformations of the different isomers of butanol over the partition function can be calculated as the ratio between the MS-QH and the SS-QH partition functions, as indicated in eqn (14). Specifically, this ratio is the inverse of the contribution of the most stable conformer:

$$F_{\mathrm{R}}^{\mathrm{MS-QH}} = \frac{Q_{\mathrm{rv,jR}}^{\mathrm{MS-QH}}}{Q_{\mathrm{rv,jR=0}}^{\mathrm{SS-QH}}} = \frac{1}{\chi_{\mathrm{R,0}}^{\mathrm{QH}}} \tag{21}$$

where R indicates a given isomer of BuOH. These ratios for the three biobutanols are depicted in Fig. 4a (t-BuOH only presents one conformer, reason by the ratio is the unity). As expected, the ratio increases with temperature and with the number of conformers. At high temperatures, even the less stable minima have some contribution and the ratio tends to a value of equal contribution by all conformations, *i.e.*, 9 for 2-BuOH and i-BuOH and 29 for n-BuOH (Table 2).

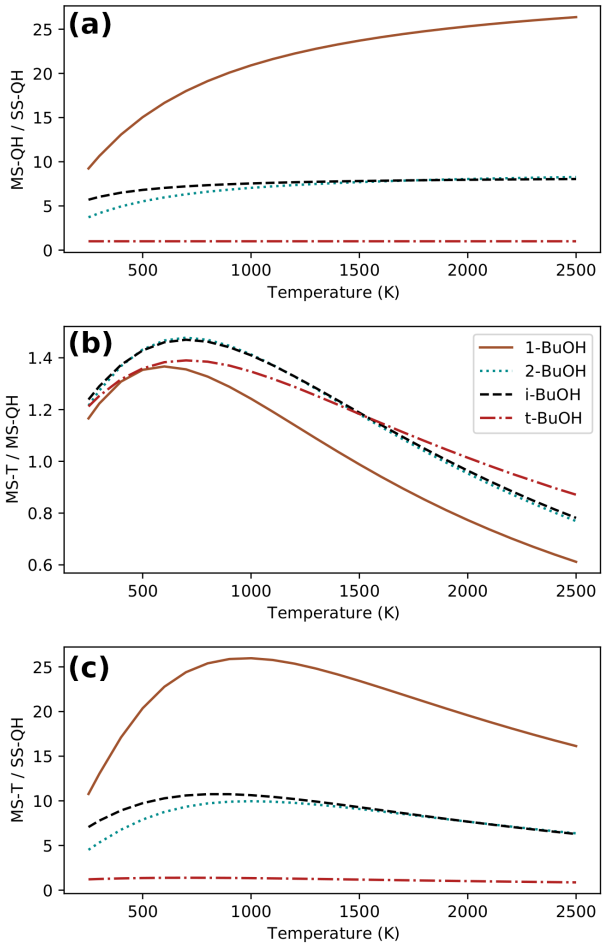

Fig. 4 Plot of the (a) multistructural, (b) torsional ananharmonic, and (c) multistructural torsional anharmonic factors for the four isomer of butanol.

The multistructural anharmonic factor, besides of the effect of multiple conformers contains the torsional anharmonic factor, plotted in Fig. 4b for the four isomers of butanol. It behaves similarly for the four species, that is, it increases with temperature until reaching a maximum at about 700 K. After that, the ratio decreases, reaching values smaller than the unity at high temperatures. This is due to the fact that the density of states of the hindered rotor partition function declines with increasing temperature whereas it remains constant for the harmonic oscillator. It is also noteworthy to mention that 2-BuOH and i-BuOH display similar behaviors, which is probably due to the fact that they present a similar skeleton. In the case of the transition states, similar trends are observed (see ESI). The final contribution of multiple structures and torsional anharmonicity is plotted in Fig. 4.

The total effect of the multistructural and torsional anharmonicity over the HA reactions, eqn (12), is plotted in Fig 5. Taking into account that the torsional anharmonicity behaves similarly for the reactants and the transition states, the main deviations from the unity are due to the peculiarities of the confor-

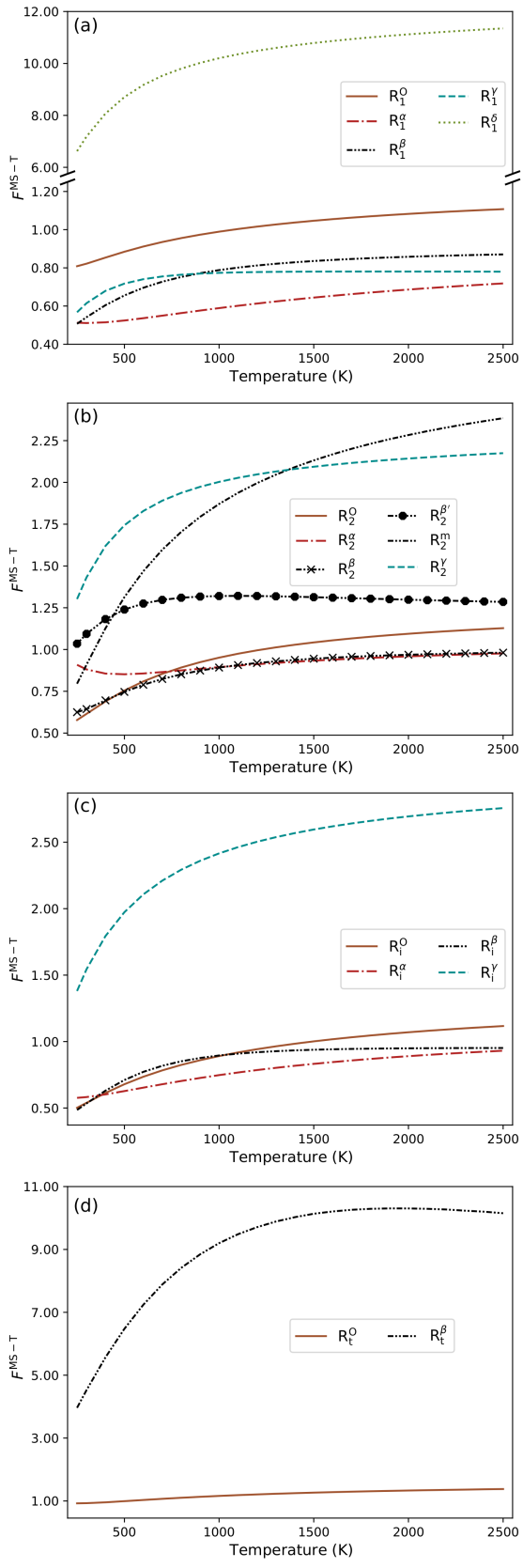

Fig. 5 Ratio between the multistructural torsional anharmonic factors for the different TSs belonging to a CRC and (a) 1-butanol, (b) 2-butanol, (c) iso-butanol, and (d) tert-butanol, plotted at different temperatures.

mational wealth. For instance, the HA from the methyl groups in 2-BuOH and i-BuOH leads to a $F^{\mathrm{MS-T}}$ factor close to three at high temperatures. Specifically, the internal rotation of the methyl group produces three indistinguishable configurations at the reactants, but the HA at the transition state structures make them distinguishable.

In the case of t-BuOH, the factor reaches a value about 9, as there is just one equilibrium structure and 9 transition state conformers. The somewhat disconcerting multistructural factor for reaction R_1^δ, larger than 3 even at low temperatures, is due to the energy distribution of the transition state conformers. The transition state structure with the lowest electronic energy (the one considered to evaluate the single-structure partition function) switches place with another structure when the ZPE is incorporated, producing an unusually high factor.

Hydrogen abstraction from secondary carbon atoms and from oxygen leads to multistructural factors that are smaller than the unity at low temperatures because the energy distribution of the conformers is different for the reactant and transition state species. In particular, several conformers contribute to the multistructural partition function of the equilibrium species but very few to the corresponding transition states.

In summary, the behavior of the multistructural factor cannot be *a priori* predicted, and a knowledge of the conformational energetics is required. Therefore, the evaluation of multistructural partition functions in flexible structures is crucial and should be preferred over single-structural calculations.

Thermal rate constants

The rate constants calculated by the MP-CVT/SCT method include an average transmission coefficient that encapsulates two dynamical contributions: tunneling and variational effects (recrossing).

For HA reactions, tunneling is significant at low temperatures, an expected result for reactions in which a light particle is being transferred. The transition states are 'tight' with imaginary frequencies ranging from $1000i$ to $1400i$ cm^{-1} for the abstraction from the carbon atoms and about $1675(\pm 30)i$ cm^{-1} for the abstraction from the oxygen atoms. The importance of this quantum effect is especially notorious for the channel associated to the HA at the hydroxyl group, with values of the transmission coefficient ranging from 80 to 135 at 250 K.

Variational effects are present in most of the studied reactions mainly at low temperatures. In all cases, the variational effects appear as a sudden increase of the ZPE (and of the vibrationally adiabatic potential) near the transition state in the forward direction toward products at $s \approx +0.10$ Bohr. In this region of the MEP the vibrational normal mode that corresponds to the approaching of the donor and acceptor atoms increases rapidly because of the formation of the hydrogen-hydrogen bond in its first stages.

Above 500 K (Fig. 6), the ratio between $\langle\gamma\rangle^{\mathrm{CVT/SCT}}$ and $\gamma_0^{\mathrm{CVT/SCT}}$ for all reaction channels is in the (0.9,1.1) interval. This means that above that temperature, the recrossing and tunneling effects of all TS conformers of a given channel can be approximated within a 10% to that of the corresponding lowest energy transition state. This fact can save a significant amount of time in

future researches, as it indicates that the MS-CVT/SCT approximation to the rate constants would lead to similar results than the MP-CVT/SCT one for these types of reactions at the temperatures of interest in combustion.

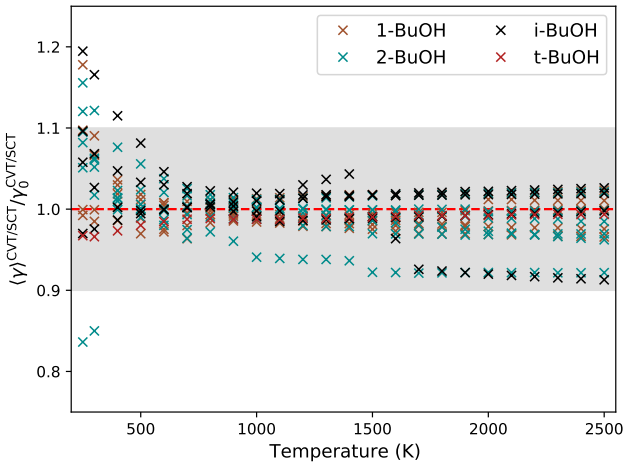

Fig. 6 Plot that shows the variation of the $\langle\gamma\rangle^{CVT/SCT}/\gamma_0^{CVT/SCT}$ ratio with temperature. Each of the CRCs is represented by a cross.

The MP-CVT/SCT rate constants were fitted (Table 4) to the analytical expression proposed by Zheng and Truhlar:[81]

$$k = A\left(\frac{T}{T_r}\right)^n \exp\left(-B\frac{T+T_0}{T^2+T_0^2}\right) \tag{22}$$

where A, B, n and T_0 are fitting parameters and T_r is a reference temperature, which in this work was set to 300 K. Equation (22) was designed to provided a better fit to thermal rate constants in reactions that present substantial quantum effects at low temperatures. This is because tunneling substantially curves the Arrhenius plot (a representation of $\log k$ versus $1/T$), which is a straight line in the Arrhenius equation.

Equation (22) also describes well the variation of the activation energy (E_a) with temperature, which is a constant in the Arrhenius equation. Considering eqn (22), E_a is given by:

$$E_a = -R\frac{d\ln k}{d(1/T)} = \left(B\cdot\frac{T^4+2T_0T^3-T_0^2T^2}{(T^2+T_0^2)^2}+nT\right)\cdot R \tag{23}$$

where R is the ideal gas constant.

Although Table 4 lists the overall rate constant for the HA from each isomer and the individual fittings to each abstraction site, in combustion chemistry is common to organize the HA rate constants by classes. Such classification depends on the type of carbon atom (primary, secondary, and tertiary) and how close it is from the oxygen atoms (C_α, C_β, etc.) Thus, the HA from the primary C_α atom of 1-BuOH will be very similar to that of i-BuOH, but quite different from that of the secondary C_α of 2-butanol. At low temperatures there is some correlation between the type of the abstraction site and the corresponding activation energy (see Table 5). As expected, the channels for the HA at C_α present

Table 4 Fitting parameters for the HA reaction rate constants. A is given in $cm^3molecule^{-1}s^{-1}$, B and T_0 are in K and n is dimensionless. Reference temperature for eqn (22) is $T_r = 300K$. The overall rate constants for isomers Z(=1, 2, i, t) of BuOH are given by R_Z^{all}.

Reaction	$A\cdot10^{12}$	B	n	T_0
R_1^{all}	2.027	1326.8	2.730	216.15
R_1^{α}	0.671	1035.2	2.541	175.94
R_1^{β}	1.177	1749.6	2.468	173.19
R_1^{γ}	1.225	1767.8	2.356	153.68
R_1^{δ}	0.955	2610.7	2.555	161.37
R_1^{O}	0.115	2922.8	2.907	189.41
R_2^{all}	0.527	405.9	3.219	344.94
$R_2^{\tilde{\alpha}}$	0.995	488.5	2.292	193.34
$R_2^{\tilde{\beta}}$	0.663	1638.7	2.469	187.32
$R_2^{\tilde{\beta}'}$	0.814	1676.1	2.402	167.74
R_2^{m}	0.730	3063.9	2.630	158.14
$R_2^{\tilde{\gamma}}$	1.033	2386.0	2.639	166.99
R_2^{O}	0.133	3063.6	2.858	186.61
R_i^{all}	1.054	1194.3	2.788	175.99
R_i^{α}	0.772	1177.8	2.503	177.99
R_i^{β}	2.909	1833.4	1.630	162.01
R_i^{γ}	1.619	3156.0	2.491	151.85
R_i^{O}	0.111	3074.6	2.888	189.46
R_t^{all}	5.214	3053.2	2.405	172.27
R_t^{β}	5.302	3060.2	2.374	172.34
R_t^{O}	0.105	3250.2	2.880	179.31

the smallest activation energy, followed for those channels where tertiary and secondary radicals are generated. Finally, radicals generated when abstracting the H from the O or from a primary carbon are less stable and, consequently, present the highest activation energy. Table 5 also shows the large variation of the activation energy with temperature and its average for different abstraction sites at three temperatures.

At the temperatures of combustion (usually at $T > 700$ K) tunneling effect is negligible and a good fit to the thermal rate constants can be achieved by an expression simpler than eqn (22), that is, by an equation of the type:

$$k = CT^m\exp(-D/T) \tag{24}$$

where C, D, and m are fitting parameters. Equation (24) is widely used in combustion so we also provide the values of the fitting parameter in the ESI. The reactions are classified by the type of hydrogen atom abstracted like for the activation energies of Table 5. The reported parameters may be useful in models for combustion but the errors that arise from considering several CRCs in just one fitting may be quite large. For instance, the absolute error of accommodating all primary HAs in a unique expression is about 50%, a situation that does not improve substantially even if the R_2^m and R_t^{β} are removed from the fit. The only situation in which this classification leads to small errors is for the HA from the oxygen atom. Therefore, HA reactions of all individual channels fitted to eqn (24) are also provided in the ESI. In our opinion, the averaged values obtained from the classification into classes are useful for qualitative discussions, as the paragraph above. How-

Table 5 Averaged free energies (in kcal/mol) at 250, 1000, and 2500 K classified according to the type of reaction.

HA site	$\langle E_a(250\ \mathrm{K})\rangle$	$\langle E_a(1000\ \mathrm{K})\rangle$	$\langle E_a(2500\ \mathrm{K})\rangle$	Channels
C_α, secondary	1.88	5.77	12.49	R_2^α
C_α, primary	3.12 ± 0.10	7.75 ± 0.14	15.00 ± 0.06	R_1^α, R_i^α
Tertiary carbon	4.20	7.73	12.16	R_i^β
Secondary carbon	4.21 ± 0.28	9.02 ± 0.12	15.85 ± 0.22	R_1^β, R_1^γ, R_2^β, $R_2^{\beta'}$
At OH	6.33 ± 0.31	13.37 ± 0.26	21.24 ± 0.22	R_1^O, R_2^O, R_i^O, R_t^O
Primary carbon	6.54 ± 0.66	12.03 ± 0.64	18.94 ± 0.56	R_1^δ, R_2^m, R_2^γ, R_i^γ, R_t^β

ever, they seldom capture the subtleties of the chemical environment generated by different isomers and this may have an impact on relative quantities like the branching ratios. Therefore, we do not recommend clustering rate constants if accurate values are pursued.

Our total MP-CVT/SCT thermal rate constants are in very good agreement with the results of Sarathy *et al.*[31] for 1-BuOH and i-BuOH (Fig. 7). For 2-BuOH our results are between the two available experimental data and for t-BuOH they are slightly lower than the experiment. There is a substantial disagreement with the experiments of Moss *et al.*[37] for the three biofuels. The rate constants employed in the combustion models of Cai *et al.*[39] (based on the HA reactions of Ref. 38) and Pelucchi *et al.*[41] substantially underestimate the total HA from 1-butanol.

The effect of the variational and tunneling effects, as well as the incorporation of multiple conformers over the total rate constant is displayed in Fig. 8. Specifically, it displays a comparison between the total MP-CVT/SCT thermal rate constants and single- or multi-structure versions of TST and CVT rate constants for the isomers of butanol. As shown in the ESI the variational effects are not large (as expected from reactions with tight TSs), so the main factors affecting the HA rate constants are tunneling and conformational flexibility. Both SS-TST and MS-TST are inadequate at low temperatures because tunneling is significant below $T = 500$ K; SS-CVT/SCT corrects for tunneling and variational effects employing the information of the TS of lowest energy, so the results improve substantially with respect to SS-TST. In spite of the improvements, single-structure approximations are unsatisfactory to study flexible molecules because: (i) it is difficult to assess 'a priory' their accuracy if calculations with multiple conformations are unavailable, and (ii) the effort to find the most stable conformer is near the same than that of finding all conformers. However, MS-CVT/SCT is accurate in all the temperatures interval and MS-TST is accurate above $T \approx 1000$ K. The accuracy of MS-TST can be improved up to temperatures above $T \approx 500$ K by using a one-dimensional tunneling correction, which does not require the evaluation of the MEP and that is accurate if tunneling is not large.

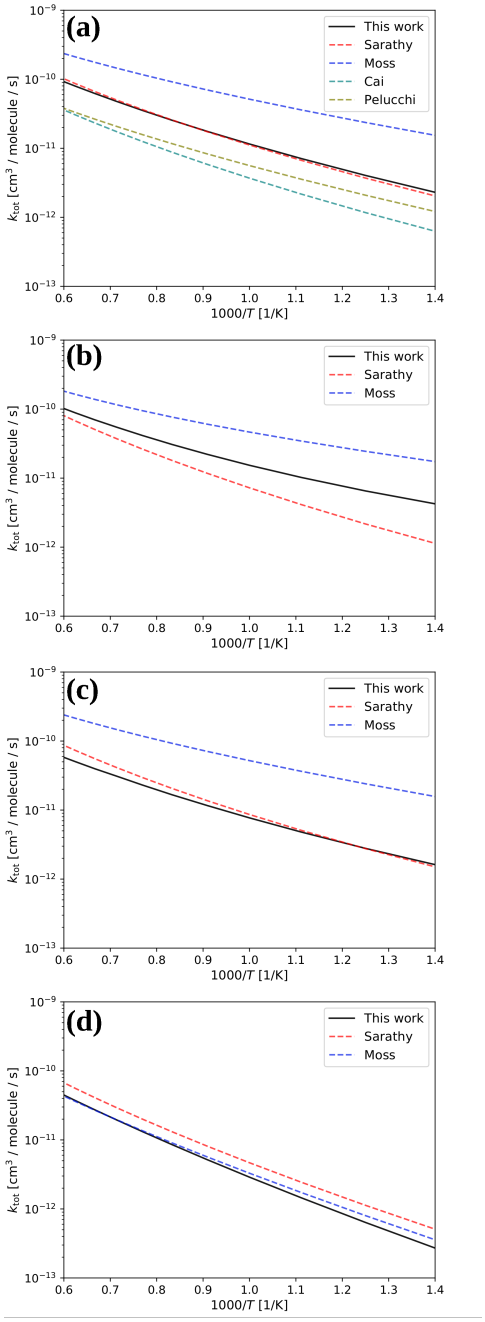

Fig. 7 Arrhenius plot of the total thermal rate constants calculated in this work and different experimental data in the T-interval 700-1600 K for (a) 1-BuOH, (b) 2-BuOH, (c) i-BuOH and (d) t-BuOH.

Product branching ratios

The branching ratios, calculated as the quotient between the HA rate constant from the oxygen or carbon sites and the total rate constant, provide the relative selectivity of each reaction channel. Their dependence with temperature can be found plotted in the ESI.

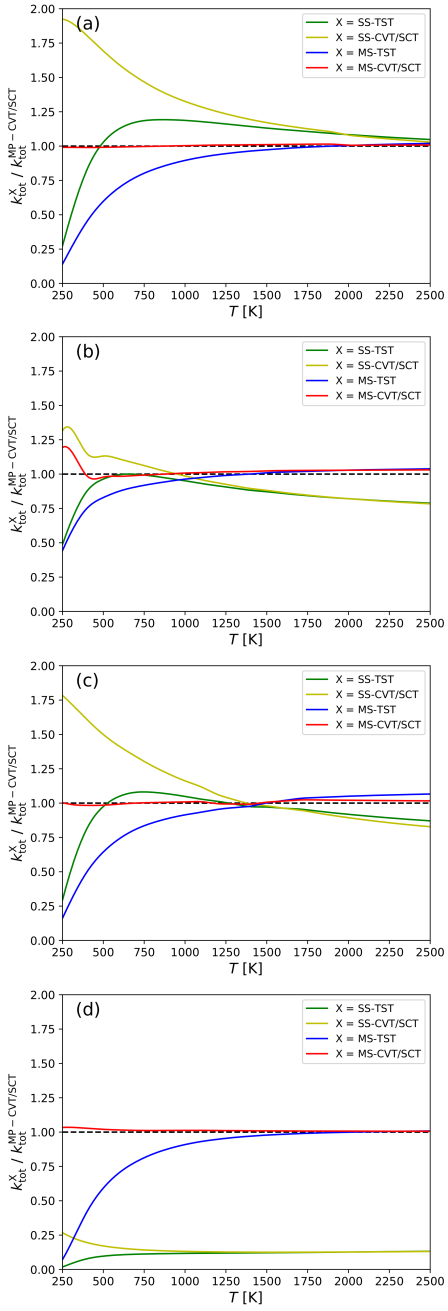

Fig. 8 Ratio between the overall HA thermal rate constants evaluated by different TST and VTST approximations with regard to the MP-CVT/SCT ones in the T-interval 250-2500 K for (a) 1-BuOH, (b) 2-BuOH, (c) i-BuOH and (d) t-BuOH.

Regarding biobutanols, the HA at C_α is, in general, the predominant channel. At low temperatures this behavior is accentuated and this channel can be considered exclusive for the 1-BuOH and 2-BuOH isomers. On the contrary, for i-BuOH, R_i^β competes with R_i^α due to the fact that this HA leads to a tertiary radical, characterized by an activation energy that is smaller than that found for other C_β biobutanol radicals. We highlight that, although HA reactions at the oxygen atom are characterized by large tunneling transmission coefficients at low temperature, their rate constants are, in general, negligible.

At high temperatures, the contribution of the other HA reactions increases to such an extent that almost all CRCs contribute significantly to the reaction mechanism. Interestingly, HA channels at methyl and hydroxyl groups present close activation energies although the importance of the former stands out significantly. The difference rests on entropic grounds: HAs at methyl groups show greater conformational wealth. Thus, whereas the HA at methyl groups can compete with other channels, the HA at the hydroxyl group is less important. A good example of this can be found in t-BuOH, where the HA can only take place at methyl groups and at the hydroxyl group. The HA at the methyl group is the dominant channel, with a branching ratio over 94% in the whole temperature range.

The branching ratios for $T = 1300$ K are shown in Fig. 9 . Our calculations and the combustion models coincide very well in the case of t-BuOH, but there are some discrepancies for the three bioalcohols. As expected, the minority channel in all cases is R_Z^O with contributions of less than 10%. Our calculations show that HA from C_α is dominant with contributions between 30 to 50% to the total rate constant. From a qualitative point of view, our results agree with those of Moss *et al.* but from a quantitative point of view differ substantially, as they report a contribution of the R^α channels larger than 80%, whereas in our calculations this percentage is only obtained below $T = 400$ K for 1-BuOH, below $T = 700$ K for 2-BuOH, and below $T = 300$ K for i-BuOH. From a quantitative point of view, the MP-CVT/SCT branching ratios for 1-BuOH agree well with those of Pelucchi *et al.* and Cai *et al.*, whereas the agreement with Sarathy *et al.* is slightly worse. The latter favors other channels than R^α at $T = 1300$ K, not only for 1-BuOH, but also for the other bioalcohols, being R_2^β, and R_i^γ the main reaction channels for 2-BuOH, and i-BuOH, respectively.

The results of the Sarathy *et al.* model for 2-BuOH also indicate that although R_2^β is the main channel, it is closely followed by R_2^γ, and R_2^m. However, the differences in the barrier heights between a hydrogen abstraction from C_α or from C_m are about 8 kcal/mol, a difference that can be hardly compensated by other factors.¶ In our work R_2^m contributes about 5% and the contribution of the R_2^γ is about three times larger; however in the combustion models both of them are considered to have the same rate constant.

Our results indicate that for 1-BuOH the R_1^α channel dominates below 1800 K. For the R_2^α channel, the C_α abstraction remains also dominant at temperatures $T < 1900$ K; above this temperature, the abstraction at the C_β, *i.e.* $R_2^\beta + R_2^{\beta'}$, dominates. Finally

¶ This excludes tunneling, which has a neglegible contribution at $T = 1300$ K

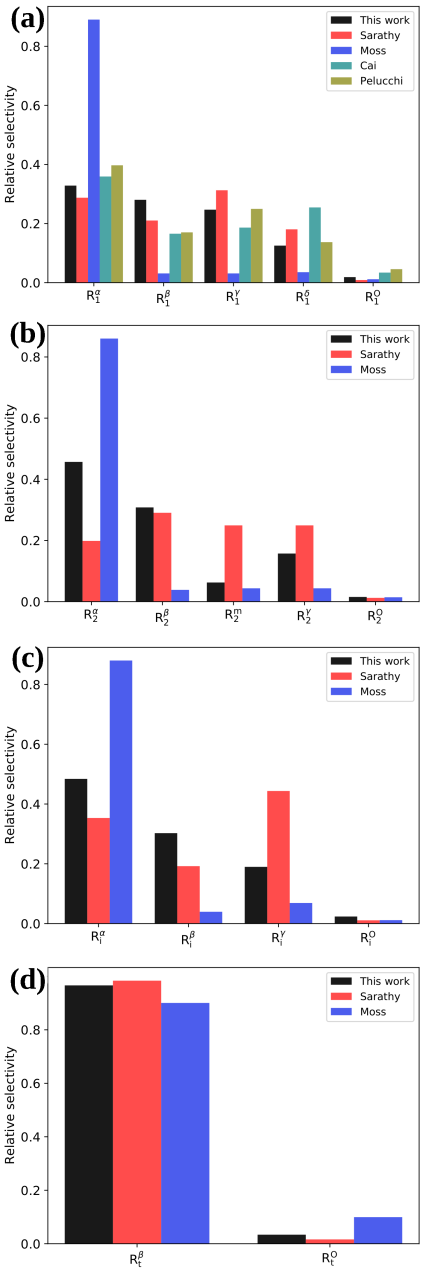

Fig. 9 Branching ratios calculated in this work and comparison with experimental data at $T = 1300$ K for (a) 1-BuOH, (b) 2-BuOH, (c) i-BuOH and (d) t-BuOH.

for i-BuOH, the R_i^α channel is always majority below 2500 K. In spite of pointing towards R^α as the main channel, our calculated rate constants show a common trend with the work of Sarathy *et al.*, specifically, that the contribution of other HA channels from carbon atoms are significant and should be taken into account in the combustion models.

5 Conclusions

In this work, we have presented an integrated protocol that allowed us to study hydrogen abstraction reactions by atomic hydrogen in a wide range of temperatures. It was designed to analyze systems with conformational flexibility and a variety of abstraction sites. The protocol incorporates a battery of programs that, together with electronic structure calculations, performs a conformational search, incorporate torsional and ZPE anharmonicities to the rovibrational partition functions, and evaluates thermal rate constants and branching ratios by the multipath canonical variational transition state theory with multidimensional small-curvature corrections for tunneling.

The protocol was applied to the hydrogen abstraction reactions by the hydrogen radical in the four isomers of butanol between 250 and 2500 K. All hydrogen abstraction sites were included in the computational treatment and reported as analytical expresions for the whole range of temperatures.

For the three biobutanols at low temperatures, the abstraction at C_α is the dominant channel. The contribution of the other channels increments with temperature to such an extent that most of them compete with the C_α abstraction at high temperatures.

Finally, we highlight that for the reactions here studied, the MS-CVT/SCT approximation is an adequate method, within a 10% error when compared to MP-CVT/SCT calculations, at the temperatures of interest in combustion. Its 'reduced' computational cost makes MS-CVT/SCT a desirable option for future research in similar systems. For combustion reactions, even a more economical approach as MS-TST, which avoids evaluation of the MEP, may suffice.

Conflicts of interest

There are no conflicts to declare.

Acknowledgements

The authors thank "Centro de Supercomputación de Galicia" (CESGA) for the use of their computational facilities. This work was partially supported by the Consellería de Cultura, Educación e Ordenación Universitaria (Centro singular de investigación de Galicia acreditación 2019-2022, ED431G 2019/03 and Grupo de referencia competitiva ED431C 2021/40) and the European Regional Development Fund (ERDF), and the Ministerio de Ciencia Inovación through Grant PID2019-107307RB-I00. M.N.D.S.C. received financial support from FCT –Fundação para a Ciência e Tecnologia, through funding for the project PTDC/QUI-QIN/30649/2017. M.N.D.S.C. would like to thank also the FCT support to LAQV-REQUIMTE (UID/QUI/50006/2020). D.F.-C. thanks Xunta de Galicia for financial support through a postdoctoral grant (modalidade A, 2017).

Notes and references

1 Q.-D. Wang and Z.-W. Liu, *J. Phys. Chem. A*, 2018, **122**, 5202–5210.

2 A. Ratkiewitcz, J. Bieniewska and T. N. Truong, *Int. J. Chem. Kinet.*, 2010, **43**, 78–98.

3 P. D. Paraskevas, M. K. Sabbe, M.-F. Reyniers, G. Papayannakos and G. B. Marin, *J. Phys. Chem. A*, 2014, **118**, 9296–9309.

4 H. Eyring, *J. Chem. Phys.*, 1935, **3**, 107–115.

5 J. Zheng, T. Yu, E. Papajak, I. M. Alecu, S. L. Mielke and D. G. Truhlar, *Phys. Chem. Chem. Phys.*, 2011, **13**, 10885–10907.

6 J. Zheng, T. Yu and D. G. Truhlar, *Phys. Chem. Chem. Phys.*, 2011, **13**, 19318–19324.

7 J. Zheng and D. G. Truhlar, *J. Chem. Theory Comput.*, 2013, **9**, 1356–1367.

8 J. Zheng and D. G. Truhlar, *Faraday Discuss.*, 2012, **157**, 59–88.

9 R. Meana-Pañeda and A. Fernández-Ramos, *J. Am. Chem. Soc.*, 2012, **134**, 346–354; (E) 134 (2012) 7193.

10 T. Yu, J. Zheng and D. G. Truhlar, *J. Phys. Chem. A*, 2012, **116**, 297–308.

11 J. L. Bao, P. Sripa and D. G. Truhlar, *Phys. Chem. Chem. Phys.*, 2016, **18**, 1032–1041.

12 J. L. Bao and D. G. Truhlar, *Chem. Soc. Rev.*, 2017, **46**, 7548–7596.

13 D. G. Truhlar, A. D. Isaacson and B. C. Garrett, in *Theory of chemical reaction dynamics*, ed. M. Baer, CRC, Boca Raton, FL, 1985, vol. 4, ch. 2, pp. 65–137.

14 A. Fernández-Ramos, A. Ellingson, B. C. Garrett and D. G. Truhlar, *Rev. Comput. Chem.*, 2007, **23**, 125–262.

15 B. C. Garrett and D. G. Truhlar, *J. Phys. Chem.*, 1979, **83**, 1052–1078.

16 B. C. Garrett and D. G. Truhlar, *J. Chem. Phys.*, 1979, **70**, 1593–1598.

17 R. T. Skodje, D. G. Truhlar and B. C. Garrett, *J. Chem. Phys.*, 1982, **77**, 5955–5976.

18 Y.-P. Liu, G. C. Lynch, T. N. Truong, D.-h. Lu and D. G. Truhlar, *J. Am. Chem. Soc.*, 1993, **115**, 2408–2415.

19 R. Meana-Pañeda and A. Fernández-Ramos, *J. Chem. Phys.*, 2014, **140**, 174303.

20 D. Ferro-Costas, E. Martínez-Núñez, J. Rodríguez-Otero, E. Cabaleiro-Lago, C. M. Estévez, B. Fernández, A. Fernández-Ramos and S. A. Vázquez, *J. Phys. Chem. A*, 2018, **122**, 4790–4800.

21 S. N. Elliott, K. B. Moore III, A. V. Copan, M. Keçeli, C. Cavallotti, Y. Georgievskii, H. F. Schaefer and S. J. Klippenstein, *Proc. Combust. Inst*, 2021, **38**, 375–384.

22 K. B. Moore III, A. V. Copan, S. N. Elliott, Y. Georgievskii, C. Cavallotti, M. Keceli and S. J. Klippenstein, AutoMech. https://github.com/Auto-Mech, 2020.

23 E. Martínez-Núñez, G. L. Barnes, D. R. Glowacki, S. Kopec, D. Peláez, A. Rodríguez, R. Rodríguez-Fernández, R. J. Shannon, J. J. P. Stewart, P. G. Tahoces and S. A. Vázquez, *J. Comput. Chem.*, 2021, **42**, 2036–2048.

24 P. L. Bhoorasigh, B. L. Slakman, F. S. Khanshan, J. Y. Cain and R. H. West, *J. Phys. Chem. A*, 2017, **121**, 6896–6904.

25 C. Cavallotti, M. Pelucchi, Y. Georgievskii and S. J. Klippenstein, *J. Chem. Theory Comput.*, 2019, **15**, 1122–1145.

26 R. Van de Vijver and J. Zádor, *Comput. Phys. Commun.*, 2020, **248**, 106947.

27 C. W. Gao, J. W. Allen, W. H. Green and R. H. West, *Comput. Phys. Commun.*, 2016, **203**, 212–225.

28 R. M. Zhang, X. Xu and D. G. Truhlar, *Comput. Phys. Commun.*, 2022, **270**, 108140.

29 S. M. Sarathy, S. Vranckx, K. Yasunaga, M. Mehl, P. Oßwald, W. K. Metcalfe, C. K. Westbrook, W. J. Pitz, K. Kohse-Höinghaus, R. X. Fernandes and H. J. Curran, *Combust. Flame*, 2012, **159**, 2028–2055.

30 P. S. Nigam and A. Singh, *Prog. Energy Combust. Sci.*, 2011, **37**, 52–68.

31 S. M. Sarathy, P. Oßwald, N. Hansen and K. Kohse-Höinghaus, *Prog. Energy Combust. Sci.*, 2014, **44**, 40–102.

32 J. Moc and J. M. Simmie, *J. Phys. Chem. A*, 2010, **114**, 5558–5564.

33 J. Zheng, G. A. Oyedepo and D. G. Truhlar, *J. Phys. Chem. A*, 2015, **119**, 12182–12192.

34 D. Katsikadakos, Y. Hardalupas, A. M. K. P. Taylor and P. A. Hunt, *Phys. Chem. Chem. Phys.*, 2012, **14**, 9615–9629.

35 J. L. Bao, R. Meana-Pañeda and D. G. Truhlar, *Chem. Sci.*, 2015, **6**, 5866–5881.

36 T. N. Truong, *J. Chem. Phys.*, 2000, **113**, 4957–4964.

37 J. T. Moss, A. M. Berkowitz, M. A. Oehlschlaeger, J. Biet, V. Warth, P.-A. Glaude and F. Battin-Leclerc, *J. Phys. Chem. A*, 2008, **112**, 10843–10855.

38 M. R. Harper, K. M. Van Geem, S. P. Pyl, G. B. Marin and W. H. Green, *Combust. Flame*, 2011, **158**, 16–41.

39 J. Cai, L. Zhang, Z. Wang, Z. Cheng, W. Yuan and F. Qi, *Energy Fuels*, 2012, **26**, 5550–5568.

40 J. Cai, L. Zhang, J. Yang, Y. Li, L. Zhao and F. Qi, *Energy*, 2012, **43**, 94–102.

41 M. Pelucchi, S. Namysl, A. Rodriguez, C. Rizzo, K. P. Somers, y. Zhang, O. Herbinet, H. J. Curran, F. Battin-Leclerc and T. Faravelli, *Energy Fuels*, 2020, **34**, 14688–14707.

42 J. A. Pople, A. P. Scott, M. W. Wong and L. Radom, *Isr. J. Chem.*, 1993, **33**, 345–350.

43 J. Merrick, D. Moran and L. Radom, *J. Phys. Chem. A*, 2007, **111**, 11683–11700.

44 I. M. Alecu, J. Zheng, Y. Zhao and D. G. Truhlar, *J. Chem. Theory Comput.*, 2010, **6**, 2872–2887.

45 K. M. Kuhler, D. G. Truhlar and A. D. Isaacson, *J. Chem. Phys.*, 1996, **104**, 4664–4671.

46 J. Bloino, M. Biczysko and V. Barone, *J. Chem. Theory Comput.*, 2012, **8**, 1015–1036.

47 T. C. Allison and D. G. Truhlar, in *Testing the accuracy of practical semiclassical methods: Modern methods for multidimensional dynamics computations in Chemistry*, ed. D. L. Thompson, World Scientific, Singapore, 1998, pp. 618–712.

48 J. Pu and D. G. Truhlar, *J. Chem. Phys.*, 2002, **117**, 1479–1481.

49 T. Yu, J. Zheng and D. G. Truhlar, *Chem. Sci.*, 2011, **2**, 2199–2213.

50 D. Ferro-Costas and A. Fernández-Ramos, *Front. Chem.*, 2020, **8**, 16.

51 D. Ferro-Costas, I. Mosquera-Lois and A. Fernández-Ramos, *J. Cheminformatics*, Under review; Download from: `https://www.researchsquare.com/article/rs-435544/v1`.

52 J. S. Binkley, J. A. Pople and W. J. Hehre, *J. Am. Chem. Soc.*, 1980, **102**, 939–947.

53 Y. Zhao, B. J. Lynch and D. G. Truhlar, *J. Phys. Chem A*, 2004, **108**, 6908–6918.

54 W. J. Hehre, R. Ditchfield and J. A. Pople, *J. Chem. Phys.*, 1972, **56**, 2257–2261.

55 Y. Zhao, N. E. Schultz and D. G. Truhlar, *J. Chem. Theory Comput.*, 2006, **2**, 364–382.

56 S. Kannath, P. Adamczyk, D. Ferro-Costas, A. Fernández-Ramos, D. T. Major and A. Dybala-Defratyka, *J. Chem. Theory Comput.*, 2020, **16**, 847–859.

57 T. B. Adler, G. Knizia and H.-J. Werner, *J. Chem. Phys.*, 2007, **127**, 221106.

58 R. A. Kendall, T. H. Dunning Jr and R. J. Harrison, *J. Chem. Phys.*, 1992, **96**, 6796–6806.

59 M. J. Frisch, G. W. Trucks, H. B. Schlegel, G. E. Scuseria, M. A. Robb, J. R. Cheeseman, G. Scalmani, V. Barone, G. A. Petersson, H. Nakatsuji, X. Li, M. Caricato, A. Marenich, J. Bloino, B. G. Janesko, R. Gomperts, B. Mennucci, H. P. Hratchian, J. V. Ortiz, A. F. Izmaylov, J. L. Sonnenberg, D. Williams-Young, F. Ding, F. Lipparini, F. Egidi, J. Goings, B. Peng, A. Petrone, T. Henderson, D. Ranasinghe, V. G. Zakrzewski, J. Gao, N. Rega, G. Zheng, W. Liang, M. Hada, M. Ehara, K. Toyota, R. Fukuda, J. Hasegawa, M. Ishida, T. Nakajima, Y. Honda, O. Kitao, H. Nakai, T. Vreven, K. Throssell, J. J. A. Montgomery, J. E. Peralta, F. Ogliaro, M. Bearpark, J. J. Heyd, E. Brothers, K. N. Kudin, V. N. Staroverov, T. Keith, R. Kobayashi, J. Normand, K. Raghavachari, A. Rendell, J. C. Burant, S. S. Iyengar, J. Tomasi, M. Cossi, J. M. Millam, M. Klene, C. Adamo, R. Cammi, J. W. Ochterski, R. L. Martin, K. Morokuma, O. Farkas, J. B. Foresman and D. J. Fox, Gaussian 09, Revision A.02; Gaussian, Inc., Wallingford, CT, 2004.

60 F. Neese, F. Wennmohs, U. Becker and C. Ripliger, *J. Chem Phys.*, 2020, **152**, 224108.

61 M. A. Ríos and J. Rodríguez, *J. Comput. Chem.*, 1992, **13**, 860–866.

62 A. Fernández-Ramos, *J. Chem. Phys.*, 2013, **138**, 134112.

63 L. Simón-Carballido, J. L. Bao, T. V. Alves, R. Meana-Pañeda, D. G. Truhlar and A. Fernández-Ramos, *J. Chem. Theory Comput.*, 2017, **13**, 3478–3492.

64 D. Ferro-Costas, M. N. D. S. Cordeiro, D. G. Truhlar and A. Fernández-Ramos, *Comput. Phys. Commun.*, 2018, **232**, 190–205.

65 J. Zheng, S. L. Mielke, K. L. Clarkson and D. G. Truhlar, *Comput. Phys. Commun.*, 2012, **183**, 1803–1812.

66 J. Zheng, R. Meana-Pañeda and D. G. Truhlar, *Comput. Phys. Commun.*, 2013, **184**, 2032–2033.

67 D. Ferro-Costas, D. G. Truhlar and A. Fernández-Ramos, *Comput. Phys. Commun.*, 2020, **256**, 107457.

68 D. G. Truhlar and A. Kuppermann, *J. Am. Chem. Soc.*, 1971, **93**, 1840–1851.

69 M. Page and J. W. McIver Jr, *J. Chem. Phys.*, 1988, **88**, 922–935.

70 Y. Y. Chuang and D. G. Truhlar, *J. Phys. Chem. A*, 1998, **102**, 242–247.

71 D. Katsakadatos, C.-W. Zhou, J. M. Simmie, H. J. Curran, P. A. Hunt, Y. Hardalupas and A. M. K. P. Taylor, *Proc. Combust. Inst.*, 2013, **34**, 483–491.

72 M. A. Abdel-Rahman, T. M. El-Gogary, N. Al-Hashimi, M. F. Shibl, K. Yoshizawa and A. M. El-Nahas, *Sci. Rep.*, 2019, **9**, 15361.

73 E. Papajak, P. Seal, X. Xu and D. G. Truhlar, *J. Chem. Phys.*, 2012, **137**, 104314.

74 K. Ohno, H. Yoshida, H. Watanabe, T. Fujita and H. Matsuura, *J. Phys. Chem.*, 1994, **98**, 6924–6930.

75 R. Meana-Pañeda, D. G. Truhlar and A. Fernández-Ramos, *J. Chem. Phys.*, 2011, **134**, 0943202.

76 I. Mosquera-Lois, D. Ferro-Costas and A. Fernández Ramos, *Phys. Chem. Chem. Phys.*, 2020, **22**, 24951–24963.

77 I. M. Alecu, J. Zheng, Y. Zhao and D. G. Truhlar, *J. Chem. Theory Comput.*, 2010, **6**, 2872–2887.

78 L. Gao, J. Zheng, A. Fernández-Ramos, D. G. Truhlar and X. Xu, *J. Am. Chem. Soc.*, 2018, **140**, 2906–2918.

79 J. Zheng, R. Meana-Pañeda and D. G. Truhlar, *J. Am. Chem. Soc.*, 2014, **136**, 5150–5160.

80 L. G. Gao, D. G. Fleming, D. G. Truhlar and X. Xu, *J. Phys. Chem. Lett.*, 2021, **12**, 4154–4159.

81 J. Zheng and D. G. Truhlar, *Phys. Chem. Chem. Phys.*, 2010, **12**, 7782–7793.